

# Cortical Bilateral Adaptations in Rats Submitted to Focal Cerebral Ischemia: Emphasis on Glial Metabolism

Yasmine Nonose<sup>1</sup> · Pedro E. Gewehr<sup>1</sup> · Roberto F. Almeida<sup>1</sup> · Jussemara S. da Silva<sup>1</sup> · Bruna Bellaver<sup>1</sup> · Leo A. M. Martins<sup>1</sup> · Eduardo R. Zimmer<sup>1,2</sup> · Samuel Greggio<sup>2</sup> · Gianina T. Venturin<sup>2</sup> · Jaderson C. Da Costa<sup>2</sup> · André Quincozes-Santos<sup>1,3</sup> · Luc Pellerin<sup>4</sup> · Diogo O. de Souza<sup>1,3</sup> · Adriano M. de Assis<sup>1</sup>

Received: 11 December 2016 / Accepted: 13 February 2017 / Published online: 7 March 2017  
© Springer Science+Business Media New York 2017

**Abstract** This study was performed to evaluate the bilateral effects of focal permanent ischemia (FPI) on glial metabolism in the cerebral cortex. Two and 9 days after FPI induction, we analyze [<sup>18</sup>F]FDG metabolism by micro-PET, astrocyte morphology and reactivity by immunohistochemistry, cytokines and trophic factors by ELISA, glutamate transporters by RT-PCR, monocarboxylate transporters (MCTs) by western blot, and substrate uptake and oxidation by ex vivo slices model. The FPI was induced surgically by thermocoagulation of the blood in the pial vessels of the motor and sensorimotor cortices in adult (90 days old) male Wistar rats. Neurochemical analyses were performed separately on both ipsilateral and contralateral cortical hemispheres. In both cortical hemispheres, we observed an increase in tumor necrosis factor alpha (TNF- $\alpha$ ), interleukin-1 $\beta$  (IL-1 $\beta$ ), and glutamate transporter 1 (GLT-1) mRNA levels; lactate oxidation; and glutamate uptake and a decrease in brain-derived neurotrophic factor (BDNF) after

2 days of FPI. Nine days after FPI, we observed an increase in TNF- $\alpha$  levels and a decrease in BDNF, GLT-1, and glutamate aspartate transporter (GLAST) mRNA levels in both hemispheres. Additionally, most of the unilateral alterations were found only in the ipsilateral hemisphere and persisted until 9 days post-FPI. They include diminished in vivo glucose uptake and GLAST expression, followed by increased glial fibrillary acidic protein (GFAP) gray values, astrocyte reactivity, and glutamate oxidation. Astrocytes presented signs of long-lasting reactivity, showing a radial morphology. In the intact hemisphere, there was a decrease in MCT2 levels, which did not persist. Our study shows the bilateralism of glial modifications following FPI, highlighting the role of energy metabolism adaptations on brain recovery post-ischemia.

**Keywords** Astrocytes · Energy metabolism · Stroke · Contralateral hemisphere · Glial reactivity

**Electronic supplementary material** The online version of this article (doi:10.1007/s12035-017-0458-x) contains supplementary material, which is available to authorized users.

✉ Adriano M. de Assis  
adriano.assis@ufrgs.br

<sup>1</sup> Postgraduate Program in Biological Sciences: Biochemistry, ICBS, Universidade Federal do Rio Grande do Sul (UFRGS), Rua Ramiro Barcelos, 2600 – Anexo Santa Cecília, Porto Alegre, RS 90035-003, Brazil

<sup>2</sup> Brain Institute of Rio Grande do Sul, Pontifícia Universidade Católica do Rio Grande do Sul (PUCRS), Porto Alegre, RS 90619-900, Brazil

<sup>3</sup> Department of Biochemistry, Universidade Federal do Rio Grande do Sul (UFRGS), Porto Alegre, RS 90035-003, Brazil

<sup>4</sup> Department of Physiology, University of Lausanne, 1005 Lausanne, Switzerland

## Introduction

Stroke is responsible for significant mortality and long-term disability worldwide [1, 2]. In the USA, more than 140,000 people die each year from stroke ([www.strokecenter.org](http://www.strokecenter.org)), while most survivors need to receive continuous care due to sequelae [3, 4]. In acute ischemic stroke, the brain regions with severely impaired blood flow become rapidly and irreversibly injured and are referred to as ischemic *core* [5]. Surrounding the *core*, there is an area of constrained blood flow called ischemic *penumbra*, which presents a partially preserved energy metabolism and structural pattern. Salvage of this penumbral region is associated with neurological improvement and recovery [6, 7].

In addition to the ischemic penumbra, other brain areas might be relevant to improve outcome after stroke. Some

clinical evidence indicates that the contralateral area to the stroke region is also critical for post-stroke tissue reorganization and for compensation of impaired functions [8–10]. Nevertheless, no studies have looked into possible metabolic adaptations that might sustain these contralateral changes during the recovery phase. Improved understanding of contributing processes in the intact hemisphere is important for optimizing approaches to functional recovery after stroke [11].

Morphological changes of astrocytes in the surrounding area of infarct present a dual role, being detrimental and/or beneficial for recovery [12, 13]. Following the ischemic insult, brain astrocytes become activated and participate in brain inflammation by secreting inflammatory factors, such as tumor necrosis factor alpha (TNF- $\alpha$ ) and interleukin-1 (IL-1) [14]. Nevertheless, astrocytes also respond to ischemia with the emergence of neuroprotective and repairing functions, promoting functional recovery [15–17].

Glutamate, the main excitatory neurotransmitter in the central nervous system (CNS), is oxidized by astroglial cells at a rate much higher than other substrates [18], especially when the exogenous glutamate concentration rises [19]. Thus, it is important to note that astrocytes are able to increase the uptake of excessive extracellular glutamate upon ischemic insult [20], contributing to the attenuation of glutamatergic neurotoxicity (excitotoxicity).

Lactate, an energy substrate to brain cells, has been shown to have neuroprotective properties in *in vitro* [21–23] and *in vivo* [24, 25] hypoxic conditions. Lactate trafficking is facilitated by MCTs [26]. In the CNS, three MCTs have been characterized: MCT1, MCT2, and MCT4 [27–30]. Recent evidence suggests that cell-specific MCT expression may participate in the brain metabolic adaptations following transient ischemic insult [31].

Here, we hypothesized that both the injured and intact cortical regions might present modulations after focal ischemic damage, trying to adapt to a new metabolic situation. We assume that these changes may be implicated in the recovery process after injury through mechanisms carried out mainly by astrocytes. To test our hypothesis, we used an experimental model of permanent occlusion, since cerebral ischemia is most permanent in humans [32]. By different methodologies, we examined the modulation of astroglial metabolism in the cerebral region surrounding the ischemic lesion and in the contralateral cortex.

## Materials and Methods

### Ethics

All animal experiments were performed in accordance with the National Institutes of Health “Guide for the Care and Use of Laboratory Animals” (NIH publication no. 80-23, revised

1996) and were approved by the Federal University of Rio Grande do Sul Animal Care and Use Committee (process number 26674).

### Reagents

2,3,5-Triphenyltetrazolium chloride (TTC) was from Sigma-Aldrich (St. Louis, MO, USA). Electrophoresis reagents were from Bio-Rad Laboratories (Hercules, CA, USA), and immunoblotting reagents were from Amersham International (Little Chalfont, Bucks, UK). Polyclonal rabbit anti-rat MCT2 (#sc-50323), polyclonal rabbit anti-rat MCT4 (#sc-50329), and polyclonal rabbit anti-rat  $\beta$ -tubulin (#sc-9104) were from Santa Cruz Biotechnology (Heidelberg, Germany). Blots were revealed with an Immobilon™ Western Chemiluminescence kit (#P90720, Millipore Corp., Billerica, MA, USA). For glutamate uptake experiments, glutamic acid, L-[3,4-<sup>3</sup>H] was purchased from PerkinElmer (Boston, MA, USA). Lactic acid, L-[1-<sup>14</sup>C] sodium salt was purchased from American Radiolabeled Chemicals, Inc. (St. Louis, MO, USA). Glutamic acid, L-[<sup>14</sup>C(U)] (#NEC290E250UC) and Optiphase “Hisafe” 3 (#1200-437) scintillation liquid were purchased from PerkinElmer (Boston, MA, USA). Protein quantification was performed with the BCA Protein Assay kit from Thermo Fisher Scientific (#23227, Rockford, IL, USA) using bovine serum albumin as a standard. Brain-derived neurotrophic factor (BDNF) ELISA kit was purchased from Promega (Madison, WI, USA). An ELISA kit for TNF- $\alpha$  was purchased from PeproTech (Rocky Hill, NJ, USA). An ELISA kit for IL-1 $\beta$  was purchased from eBioscience (San Diego, CA, USA). GLAST (Rn00667869\_m1), and glutamate transporter 1 (GLT-1) (Rn00691548\_m1), and  $\beta$ -actin (Rn00570130\_m1) TaqMan primers and probes were purchased from Applied Biosystems (#4331182, Foster City). All other reagents were of analytical grade. Polyclonal rabbit anti-glia fibrillary acidic protein (GFAP) was purchased from Dako (Z0334, Glostrup, Denmark). AlexaFluor® 555 and Hoescht 33258 were purchased from Invitrogen (Carlsbad, CA, USA).

### Animals

Animals were obtained from the Central Animal House of the Department of Biochemistry, ICBS, UFRGS. Adult male Wistar rats (90–100 days old, weighing 300–350 g) were housed three to five per cage under controlled light and environmental conditions (12-h light/12-h dark cycle at temperature of 22  $\pm$  2 °C), with water and commercial food pellets available *ad libitum*.

## Induction of Focal Permanent Ischemia

The focal ischemic lesion was induced by blood thermocoagulation of pial vessels over the motor and sensorimotor cortices [33–36]. Briefly, the animals were anesthetized with ketamine hydrochloride (70 mg/kg, i.p.) and xylazine hydrochloride (10 mg/kg, i.p.) and placed in a stereotaxic apparatus. The skull was surgically exposed, and a craniotomy was performed by exposing the left frontoparietal cortex (+2 to –6 mm A.P. and –2 to –4 mm M.L. from the bregma) [37]. The blood inside the pial vessels was thermocoagulated transdurally by the apposition of a hot probe close to the dura mater. The rostrocaudal extent of the surface of the frontal and parietal cortices was lesioned. After the procedure, the skin was sutured and the body temperature was maintained at 37 °C using a heating pad until recovery from anesthesia. Animals from the sham group were only submitted to the aforementioned craniotomy. All animals with apparent surgical damage were excluded from this study.

## Cylinder Test

The cylinder test was performed to evaluate the sensorimotor performance of each animal after induction of the FPI model. The test is based on the spontaneous exploratory behavior of rodents, and it reveals forelimb preference when the animal rears to explore its environment by making forelimb contact with the cylinder walls [35]. Animals were subjected to one trial 1 day prior and again 2 and 9 days after ischemia (Fig. 1a). To prevent habituation to the cylinder, the number of movements recorded was limited to 20. The occurrences of ipsilateral (to the lesion), contralateral, or simultaneous forelimb use were counted. The symmetry score for each animal was calculated on each day by a previously described formula [38]. For the ischemic group, only animals with a symmetry score between 0 and 30% were selected for experiments.

## Experimental Procedure and Tissue Preparation

Rats were divided into two groups: sham (S) and ischemia (I). Animals were euthanized by decapitation after a short (2 days) or medium (9 days) period following surgery, and the following parameters were evaluated: *in vivo*—(1) symmetry test and (2) [<sup>18</sup>F]FDG metabolism; *ex vivo*—(3) lesion size, (4) glutamate uptake, and (5) substrate oxidation to <sup>14</sup>CO<sub>2</sub>; and *post-mortem*—(6) astrocytic reactivity, (7) glutamate transporter expression, (8) MCT immunoccontent, and (9) cytokine and trophic factor levels. For the *ex vivo* and *post-mortem* experiments, we determined a specific region of the cerebral cortex after TTC (lesion size) and micro-Pet scan, called the cerebral cortical cluster (somatosensorial, entorinal, auditive, and visual cortices). The clusters were dissected and analyzed

separately in both cerebral hemispheres (ipsilateral and contralateral cerebral cortices).

## Lesion Size Measurement

We used TTC staining to delineate the ischemic core region from the peri-infarct area (shadow zone) and to assess the infarct volume. Briefly, the brain was rapidly removed from the skull and sectioned in the coronal plane into slices of approximately 2 mm thick using a rat brain matrix ( $n = 6$ ). The slices were immersed for 30 min in a 2% TTC solution at 37 °C followed by overnight fixation in 4% paraformaldehyde (Sigma, St. Louis, MO, USA). After TTC staining, the slices were arranged in a frontal-occipital orientation and digital images were taken. Brain slices were analyzed with ImageJ software (NIH, Bethesda, MD, USA). The infarct volume was calculated with the following formula: infarct volume = [measured infarct area × slice thickness (2 mm)] + [area of contralateral corresponding structure × slice thickness] – [area of ipsilateral corresponding structure × slice thickness] [39, 40]. The results are expressed in cubic millimeters.

## Micro-PET Brain Scan

The rats were transported to the preclinical imaging facility 2 days before the micro-PET scans ( $n = 6$ ). At the three time points (1 day pre-FPI—baseline, 2 and 9 days post-FPI), the animals were individually anesthetized using a mixture of isoflurane and medical oxygen (3–4% induction dose), and an intravenous bolus injection of [<sup>18</sup>F]FDG (mean ± SD 1.05 ± 0.05 mCi) into the tail vein was made after overnight fasting (Fig. 4a). Then, each rat was returned to its home cage for a 40-min period of conscious (awake) *in vivo* metabolism of [<sup>18</sup>F]FDG. After the uptake period, each rat was placed in a head-first prone position and scanned with the Triumph™ micro-PET/CT (LabPET-4, TriFoil Imaging, Northridge, CA, USA) under inhalatory anesthesia (2–3% maintenance dose). Throughout these procedures, the animals were permanently kept on a pad heated to 36 °C. For radiotracer readings, 30-min list mode static acquisitions were acquired with the field of view (FOV; 3.75 cm) centered on the rat's head. All data were reconstructed using the maximum likelihood estimation method (MLEM-3D) algorithm with 20 iterations. Each reconstructed micro-PET image was spatially normalized into an [<sup>18</sup>F]FDG template using brain normalization in PMOD v3.5 and the Fusion Toolbox (PMOD Technologies, Zurich, Switzerland). An MRI rat brain volume of interest (VOI) template was used to overlay the normalized images previously coregistered to the micro-PET image database. Activity values were normalized for the injected dose and the animal body weight and are therefore expressed in standard uptake values (SUVs). Mean SUVs of 57 brain regions

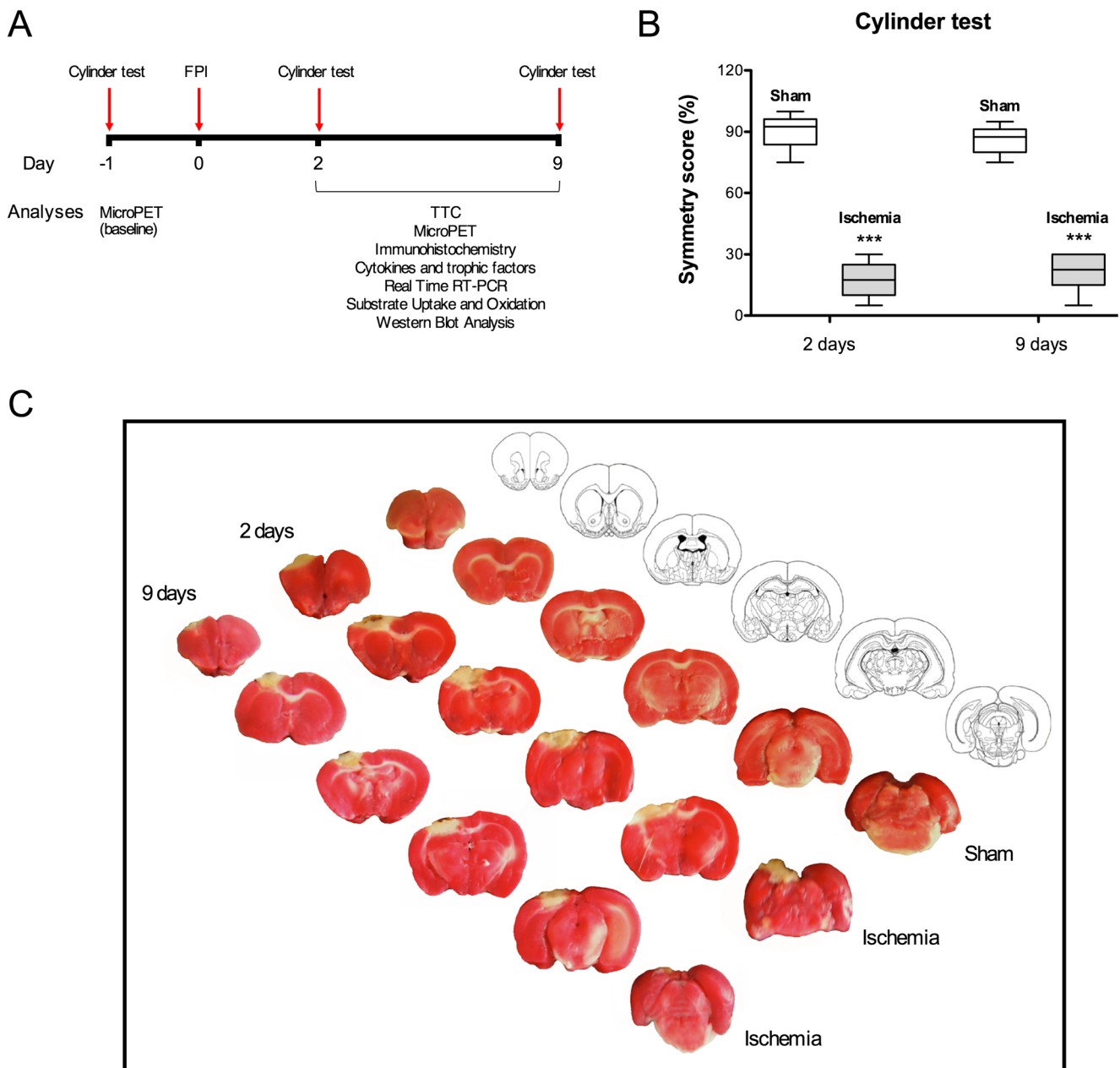


**Fig. 1** The FPI model reduced symmetry scores and produced cortical infarct, as demonstrated by TTC stain. **a** Timeline indicating the experimental design. **b** Symmetry score differences between groups 2 and 9 days following FPI; \*\*\* $P < 0.001$  (one-way ANOVA,  $n = 10$  per

group). The data are expressed as the means  $\pm$  SEM. **c** A representative TTC-stained FPI-injured brain at 2 and 9 days post-ischemia compared to a sham control. The corresponding position mapped to the bregma taken from Paxinos and Watson [37] is shown

were extracted using a predefined VOI template [41–43]. For analysis at the voxel level, MINC tools ([www.bic.mni.mcgill.ca/ServicesSoftware](http://www.bic.mni.mcgill.ca/ServicesSoftware)) were used for image processing and analysis [44].

### L-Glutamate Uptake

Slices (300  $\mu\text{m}$ , 100–120 mg;  $n = 6$ ) of cerebral cortical clusters were rapidly obtained using a McIlwain Tissue Chopper and immersed in HBSS (in mM: 137 NaCl, 0.60  $\text{Na}_2\text{HPO}_4$ ,

3.0  $\text{NaHCO}_3$ , 20 HEPES- $\text{Na}^+$ , 5.0 KCl, 0.40  $\text{KH}_2\text{PO}_4$ , 1.26  $\text{CaCl}_2$ , 0.90  $\text{MgSO}_4$ , and 5.55 glucose, pH 7.2) at 4  $^\circ\text{C}$ . Cortical slices were preincubated with HBSS at 37  $^\circ\text{C}$  for 15 min, followed by the addition of 0.33  $\mu\text{Ci}$  of L- $^3\text{H}$ -glutamate. Incubation was stopped after 7 min with two ice-cold washes of 1 mL HBSS. After washing, 0.5 N NaOH was immediately added to the slices and kept overnight.  $\text{Na}^+$ -independent uptake was measured using the aforementioned protocol with modifications of the temperature (4  $^\circ\text{C}$ ) and the composition of the medium (N-methyl-D-glucamine instead

of NaCl). Na<sup>+</sup>-dependent uptake was measured as the difference between the total uptake and the Na<sup>+</sup>-independent uptake [45]. Incorporated radioactivity was measured using a liquid scintillation counter (Hidex 300 SL, Mikrotek Laborsysteme, Overath, Germany).

### Substrate Oxidation to <sup>14</sup>CO<sub>2</sub>

Briefly, cerebral cortex cluster slices (300 μm, 100–120 mg; *n* = 6) were obtained as described above, transferred into flasks and preincubated in Dulbecco's buffer for 30 min. Before incubation with substrates, the reaction medium was gassed with a 95% O<sub>2</sub>:5% CO<sub>2</sub> mixture for 30 s. Slices were incubated in 1 mL of Dulbecco's buffer containing either (i) 10 μM L-glutamic acid + 0.2 μCi L-[<sup>14</sup>C(U)] glutamate or (ii) 10 μM sodium L-lactate + 0.2 μCi L-[U-<sup>14</sup>C] lactate. Then, flasks containing the slices were sealed with rubber caps and parafilm and incubated at 37 °C for 1 h in a Dubnoff metabolic shaker (60 cycles/min), as previously described [46]. The incubation was stopped by adding 0.2 mL 50% trichloroacetic acid through the rubber cap into the flask, while 0.1 mL of 2 N NaOH was injected into the central wells. Thereafter, flasks were shaken for an additional 30 min at 37 °C to trap CO<sub>2</sub>. Afterwards, the content of the central well was transferred to vials and assayed for CO<sub>2</sub> radioactivity in a liquid scintillation counter. All results were calculated based on the initial radioactivity in the incubation medium [47].

### RNA Extraction and Quantitative RT-PCR

To evaluate GLAST and GLT-1 expression, real-time RT-PCR was performed. Total RNA was isolated from the cerebral cortical clusters (*n* = 6) using TRIzol Reagent (Invitrogen, Carlsbad, CA). The concentration and purity of the RNA were determined spectrophotometrically at a ratio of 260/280. Then, 1 μg of total RNA was reverse-transcribed using Applied Biosystems™ High-Capacity cDNA Reverse Transcription Kit (Applied Biosystems, Foster City, CA) in a 20 μL reaction, according to the manufacturer's instructions. GLAST, GLT-1, and β-actin mRNA levels were quantified by real-time RT-PCR. Quantitative RT-PCR was performed in duplicate using the Applied Biosystems 7500 Fast system. As controls, a no-template and a no-reverse transcriptase were used in each assay, producing no detectable signal during 40 cycles of amplification. Therefore, target mRNA levels were normalized to β-actin levels using the 2<sup>-ΔΔCt</sup> method [48].

### Western Blot for MCT2 and MCT4

For protein immunoccontent evaluation, cerebral cortical clusters from sham and ischemia groups were obtained 2 or 9 days after surgery (*n* = 5). Cells were solubilized in ice-cold lysis buffer (4% SDS, 2 mM EDTA, 50 mM Tris-HCl pH 6.8), standardized in sample buffer (62.5 mM Tris-HCl pH 6.8, 2% (w/v) SDS, 5% β-mercaptoethanol, 10% (v/v) glycerol, 0.002% (w/v) bromophenol blue), and boiled at 95 °C for 5 min. Samples were separated by SDS-PAGE (10 μg protein/well) and transferred to a nitrocellulose membrane (GE Healthcare). Adequate loading of each sample was confirmed using Ponceau S staining. After blocking with 5% (w/v) skim milk overnight, membranes were incubated with primary polyclonal rabbit antibody overnight at 4 °C [MCT2, 1:200 dilution; MCT4, 1:200 dilution; and β-tubulin, 1:1000 dilution], washed and incubated with horseradish peroxidase-conjugated donkey anti-rabbit IgG (NA934V, 1:5000 dilution, GE Healthcare, UK) secondary antibody for 2 h. Chemiluminescent bands were detected in an ImageQuant LAS4000 system (GE Healthcare) using an Immobilon™ Western chemiluminescence kit (#P90720, Millipore) and quantified with ImageQuant TL software (version 8.1, GE Healthcare). The results are expressed in percent of control levels after normalization using β-tubulin as an internal standard.

### GFAP Immunohistochemistry and Astrocytic Morphological Analysis

Immunohistochemistry for GFAP-positive astrocytes was performed to evaluate morphological parameters. To confirm qualitative morphological findings, semiquantitative and quantitative evaluations were performed to estimate GFAP immunoreactivity and astrocytic processes. Briefly, brains (*n* = 6) were fixed for 24 h with 4% Paraformaldehyde (PFA) diluted in phosphate-buffered saline (PBS, pH 7.4), cryoprotected through immersion in sucrose solution (gradually, 15 to 30% until they sank) and frozen at -20 °C. Coronal brain slices (30 μm), approximately ranging (relative to bregma) from +2.20 mm (rostrally) to -0.80 mm (caudally), were obtained using a cryostat (MEV, SLEE Medical GMBH, Mainz, Germany). Brain slices were post-fixed with 4% PFA-PBS for 15 min, permeabilized in 0.1% Triton X-100 diluted in PBS (PBS-Tx) and then blocked for 1 h with 5% fetal goat serum also diluted in PBS-Tx. Histological samples were incubated for 24 h at 4 °C with polyclonal rabbit anti-GFAP (1:500 in PBS-Tx), followed by 2-h incubation with goat anti-rabbit AlexaFluor® 555 secondary antibody (1:1000 in PBS-Tx). Samples were also stained for nuclear visualization with Hoechst 33258 according to the manufacturer's instructions. Images were obtained with a Leica TCS SP5 II laser-scanning confocal microscope and acquired at 8-bit

gray-scale (256 Gy levels) using the Leica Application Suite Advanced Fluorescence software (Leica Microsystems, Munich, Germany).

The morphological analysis was made in three regions of interest (referred to as regions A, B, and C) approximately 300  $\mu\text{m}$  surrounding the cortical lesion (Fig. 3a) at 2 and 9 days post-FPI. Evaluation of cellular fluorescence intensity was performed as previously described [49] with modifications. For astrocytic ramification analysis, the Sholl's technique was applied [49, 50]. Briefly, orthogonal lines and ten virtual concentric circles with 3- $\mu\text{m}$  intervals were drawn around the analyzed astrocytes using ImageJ software (Fig. 3a). Astrocyte morphological findings were quantified as previously described [51].

### Inflammatory Response and Trophic Factor Measurements

Samples of cerebral cortical clusters ( $n = 6$ ) were homogenized in phosphate KCl buffer ( $\text{HNa}_2\text{PO}_4$  20 mM; KCl 140 mM; pH 7.4) and stored at  $-20^\circ\text{C}$  until the start of the analysis. TNF- $\alpha$  levels were measured using a rat TNF- $\alpha$  ELISA kit from Peprotech. IL-1 $\beta$  levels were measured using ELISA kits for IL-1 $\beta$  from eBioscience. The results are expressed in ng/mL. BDNF levels were measured using commercial ELISA kits from Promega. The results are expressed in ng/mL or pg/mL.

### Statistical Analysis

In micro-PET analysis, each parametric image was coregistered to a structural MRI template, images were blurred using a Gaussian kernel with a full-width half-maximum of 1.2 mm, and t-statistical maps were generated (Statistical Parametric Mapping, Rmnc, <https://github.com/Mouse-Imaging-Centre/RMINC>). In all ex vivo and post-mortem analyses, ischemic and sham brains were separated into contralateral (right) and ipsilateral (left) cortices, the latter representing the ischemic side in the ischemia group. The results from the ipsilateral and contralateral hemispheres of the ischemia group were compared to the same brain hemispheres of sham-operated controls. In addition, ischemic brains were also compared between the contralateral and the ipsilateral hemisphere to determine whether the stroke had affected both sides of the brain. The data are expressed as the means + SEM. All analyses were performed with Prism GraphPad (version 6.01 for Windows, GraphPad Software, San Diego, CA, USA, [www.graphpad.com](http://www.graphpad.com)). Differences among the groups were analyzed by one-way ANOVA followed by Bonferroni post hoc test, with levels of significance below  $P < 0.05$ .

The Z-score was calculated using the following formula:

$$Z = \frac{x - \mu}{\sigma}$$

where  $x$  is the sample value (raw score),  $\mu$  is the population mean, and  $\sigma$  is the standard deviation of the population. The absolute value of  $Z$  represents the distance between the raw score and the population mean in units of standard deviation [52].

## Results

### FPI Decreases the Symmetry Score and Produces a Significant Infarct Zone

At the cylinder test, the symmetry score decreased 2 days post-FPI, which persisted up to 9 days post-FPI (Fig. 1b), revealing a consistent motor impairment in the contralateral forelimb, as expected for the ischemia group. We did not observe forelimb preference in the sham group.

By TTC analysis, the FPI group presented a well-defined infarct zone 2 days after ischemia (Fig. 1c, visualized by pale staining,  $120 \pm 99 \text{ mm}^3$ ), which decreased at 9 days post-FPI (Fig. 1c,  $32 \pm 6 \text{ mm}^3$ ). The sham group presented no damage (Fig. 1c).

### FPI Decreases Glucose Uptake In Vivo Only in the Ipsilateral Hemisphere

Averaged SUV images showed consistent [ $^{18}\text{F}$ ]FDG brain metabolism. There was no FPI effect in the contralateral hemisphere. In the ipsilateral hemisphere, FPI decreased [ $^{18}\text{F}$ ]FDG brain uptake at three time points analyzed (baseline, 2 and 9 days post-FPI) in the [ $^{18}\text{F}$ ]FDG global uptake ( $F_{(2, 10)} = 4.229$ ,  $P = 0.03$ ), where the reduction was more pronounced 2 days after FPI compared to baseline values ( $P_{\text{adjusted}} = 0.04$ ). Analysis of anatomically delineated VOIs, designated here as cortical ischemic cluster (cortex regions: auditory + entorhinal + somatosensory + visual), presented a decrease in [ $^{18}\text{F}$ ]FDG metabolism in the ipsilateral hemisphere compared to the contralateral hemisphere 2 and 9 days post-FPI (Fig. 2c;  $P = 0.001$  and  $P = 0.010$ , respectively). A voxel-based analysis demonstrated a large unilateral cortico-hippocampal hypometabolic area in the group 2 days after FPI compared with baseline (peak  $t_{(5)} = 7.9$ ,  $P = 0.0005$ , statistical cluster volume  $367.832 \text{ mm}^3$ , Fig. 2d), but this hypometabolic area was found to be reduced 9 days after FPI (peak  $t_{(5)} = 4.8$ ,  $P = 0.005$ , statistical cluster volume  $41.184 \text{ mm}^3$ , Fig. 2e). Additionally, there was a significant recovery of glucose metabolism between 2 and 9 days

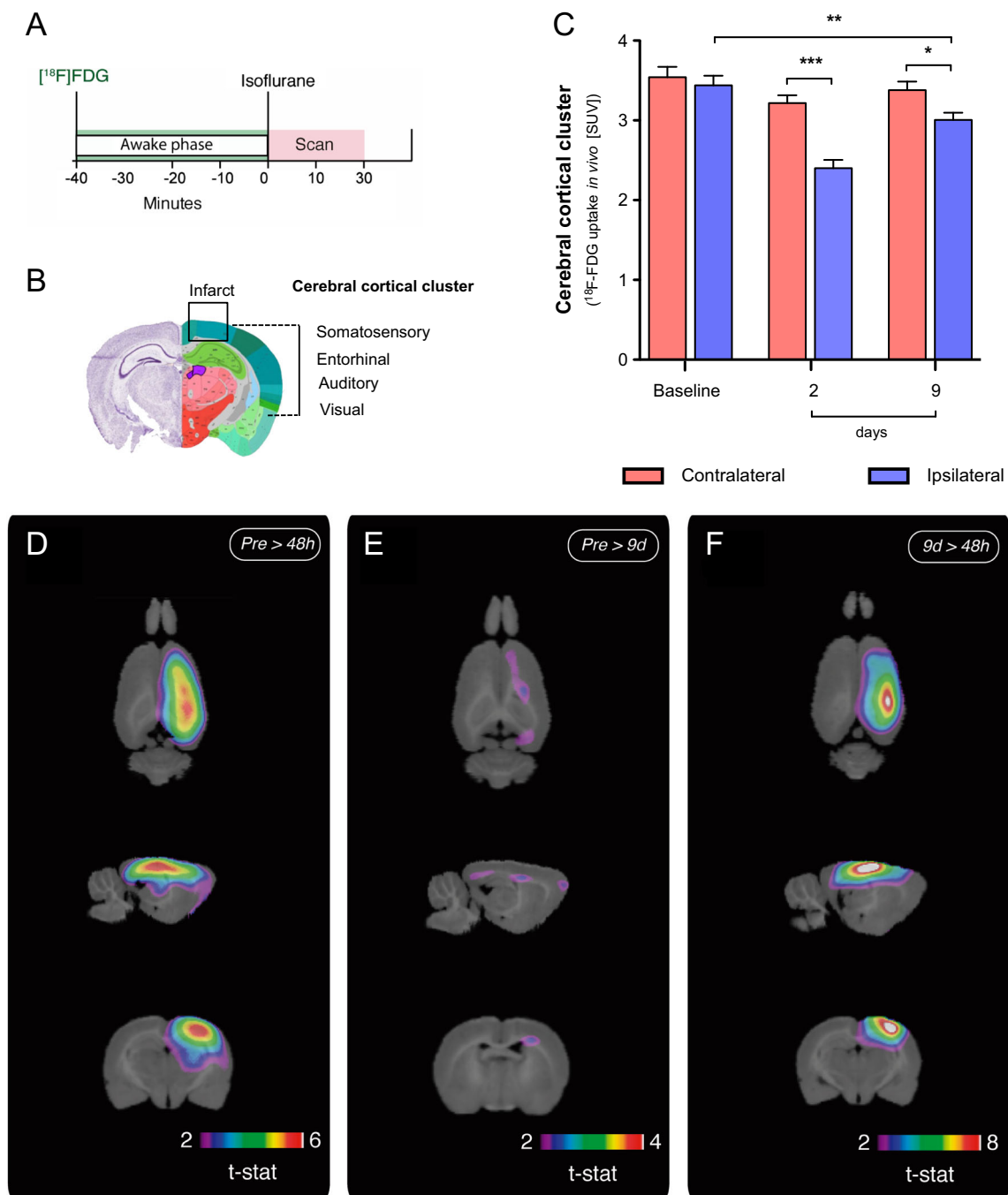


**Fig. 2** Glucose metabolism in vivo after FPI. **a** Schematic illustration of the micro-PET scan protocol. **b** Cerebral cortical cluster representing the analyzed area. **c** SUV values of [<sup>18</sup>F]FDG uptake in the cerebral cortical cluster in all times studied. **d** Comparison between baseline and 2 days post-FPI measurements of [<sup>18</sup>F]FDG metabolism. Red color represents bigger statistical significance,  $P = 0.0005$  (t-statistical map). **e** [<sup>18</sup>F]FDG uptake 9 days post-FPI, showing a hypometabolic cortical region when

compared to baseline values,  $P = 0.005$  (t-statistical map). **f** Voxel-based analyses between 2 and 9 days of [<sup>18</sup>F]FDG uptake values, demonstrating a significant recovery in the glucose metabolism accounting for the whole brain,  $P = 0.0001$  (t-statistical map). All data are expressed as the means + SEM,  $*P < 0.05$ ;  $**P < 0.01$ ;  $***P < 0.001$  (one-way ANOVA,  $n = 6$  per group) (color figure online)

based on [<sup>18</sup>F]FDG values (peak  $t_{(5)} = 10.6$ ,  $P = 0.0001$ , Fig. 2f). Nevertheless, the lesioned hemisphere did not fully recover, as a significant difference in the ipsilateral hemisphere 9 days post-FPI was observed compared with

the same hemisphere baseline [<sup>18</sup>F]FDG uptake values (Fig. 2b; I,  $3.00 \pm 0.09$ ; baseline,  $3.44 \pm 0.12$ ;  $P = 0.0063$ ). For a full description of VOIs, see Supplementary Fig. 1.

### Ischemic Injury Promotes Glial Reactivity Only in the Ipsilateral Hemisphere

Semiquantitative and quantitative analysis revealed that the regional GFAP immunofluorescence significantly increased in the ipsilateral cortex 2 days post-FPI, an effect that persisted up to 9 days (Fig. 3b, d, 2 days; ipsilateral I,  $13.22 \pm 2.054$ ; contralateral I,  $33.37 \pm 1.693$ ;  $P = 0.0016$ ; 9 days, ipsilateral I,  $44.10 \pm 4.678$ ; contralateral I,  $17.54 \pm 0.6448$ ;  $P = 0.0049$ ; Fig. 3c, 2 days, ipsilateral I,  $118.6 \pm 3.33$ ; contralateral I,

$82.45 \pm 9.74$ ;  $P = 0.0247$ ; 9 days, ipsilateral I,  $163.8 \pm 13.77$ ; contralateral I,  $70.24 \pm 1.76$ ;  $P = 0.0025$ ).

Primary processes extending from astrocytes soma were more prominent in the ischemic cerebral hemisphere than the corresponding contralateral or both cerebral hemispheres of the sham group. Ramification from primary processes (secondary processes) also increased in the ischemic groups. Sholl's analysis (Fig. 4a) showed that FPI increased the number of total primary processes in the ipsilateral hemisphere of the cerebral cortical cluster (Fig. 4b; 2 days, ipsilateral I,

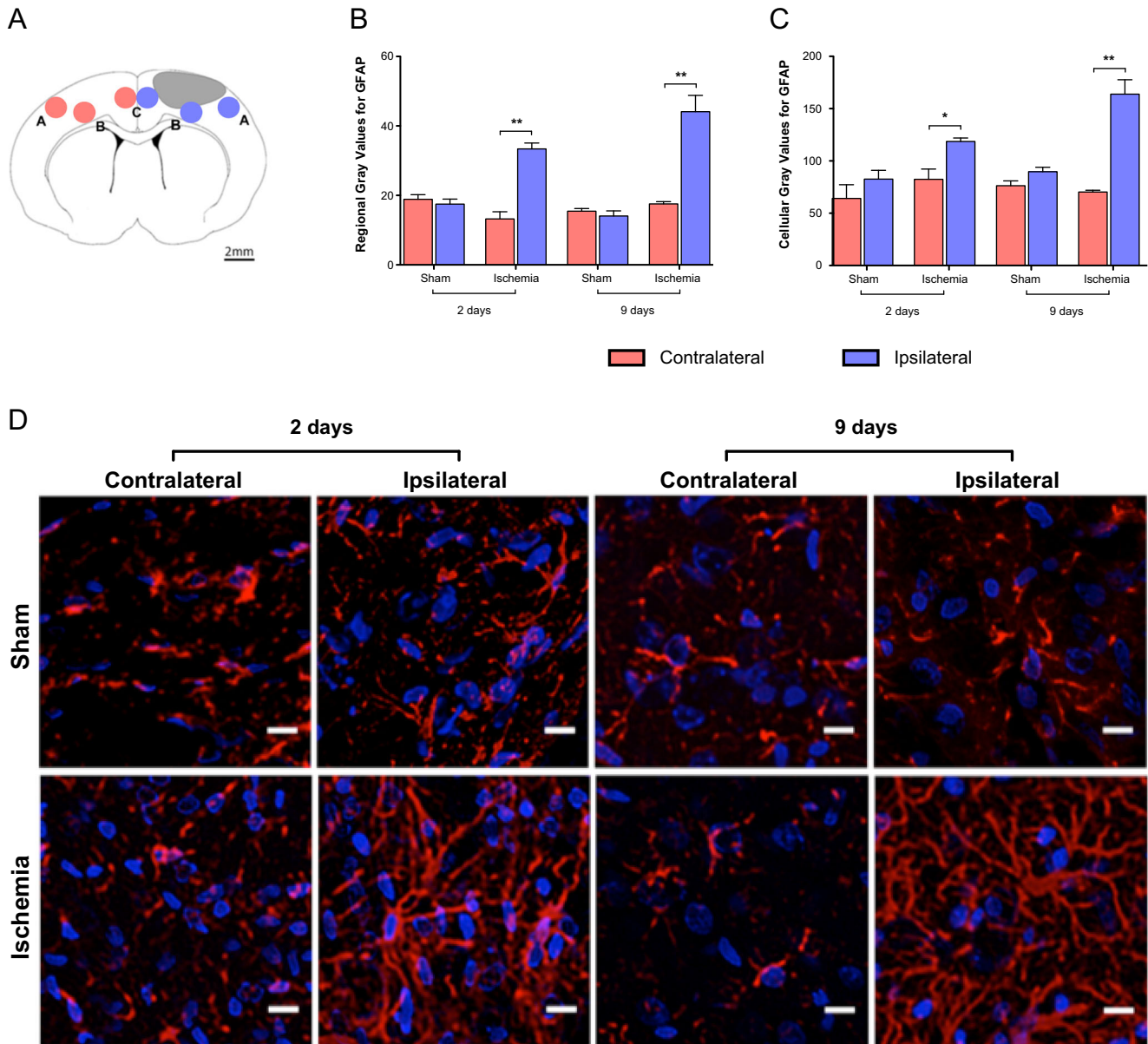


**Fig. 3** GFAP shows increased optical density in ipsilateral astrocytes post-FPI. **a** Brain slice amplified field demonstrating our regions of interest (A, B and C) (adapted from Paxinos and Watson [37]) in the ipsilateral and contralateral cortices. **b** Regional immunofluorescence for GFAP (gray values). **c** Cellular immunofluorescence of GFAP (gray

values). **d** Representative morphological changes were evident in ipsilateral astrocytes at 2 and 9 days post-FPI. All data are expressed as the means  $\pm$  SEM, \* $P < 0.05$ ; \*\* $P < 0.01$  (one-way ANOVA,  $n = 6$  per group). Scale bar 20  $\mu$ m



5.19 + 0.12; contralateral I, 3.28 + 0.24;  $P = 0.0021$ ; 9 days, ipsilateral I, 5.44 + 0.69; contralateral I, 3.11 + 0.22;  $P = 0.03$ ). As consequence, FPI increased the number of total intersections of primary processes (Fig. 4c; 2 days, ipsilateral I, 32.62 + 1.48; contralateral I, 14.39 + 1.66;  $P = 0.0012$ ; 9 days, ipsilateral I, 35.39 + 5.91; contralateral I, 12.61 + 0.49;  $P = 0.018$ ) and increased the number of total secondary processes in the ipsilateral cortex (Fig. 4d; 2 days, ipsilateral I, 3.22 + 0.72; contralateral I, 0.55 + 0.05;  $P = 0.0212$ ; 9 days, ipsilateral I, 4.33 + 0.92; contralateral I, 1.00 + 0.19;  $P = 0.0237$ ). It is worthwhile to note that the total number of primary processes and/or intersections is mainly due to an increase in the number of processes/intersections counted in central quadrants (Fig. 4e; 2 days, ipsilateral I, 2.69 + 0.14; contralateral I, 1.33 + 0.19;  $P = 0.0049$ ; 9 days, ipsilateral I, 2.83 + 0.44; contralateral I, 1.33 + 0.19;  $P = 0.0356$ ; Fig. 4f; 2 days, ipsilateral I, 18.53 + 1.51; contralateral I, 5.61 + 0.91;

$P = 0.0018$ ; 9 days, ipsilateral I, 20.11 + 3.037; contralateral I, 5.94 + 0.66;  $P = 0.0103$ ).

### Cytokine and Trophic Factor Levels in the Cerebral Cortex Were Altered by FPI

FPI significantly affected the levels of cytokines and trophic factors: (i) it increased TNF- $\alpha$  levels in both hemispheres 2 days post-FPI, an effect that persisted up to 9 days (Fig. 5a; 2 days, contralateral I, 34.02 + 2.356; S, 17.50 + 3.353;  $P = 0.0031$ ; ipsilateral I, 37.88 + 2.576; S, 9.050 + 1.951;  $P < 0.0001$ ; 9 days, contralateral I, 24.33 + 1.676; S, 15.17 + 1.189;  $P = 0.0112$ ; ipsilateral I, 18.53 + 3.624; S, 7.000 + 1.097;  $P = 0.0382$ ); and (ii) it increased IL-1 $\beta$  levels at 2 days in both hemispheres, an effect that persisted up to 9 days only in the contralateral cortex (Fig. 5b; 2 days, contralateral I, 30.88 + 1.774; S, 19.30 + 3.843;  $P = 0.0151$ ;

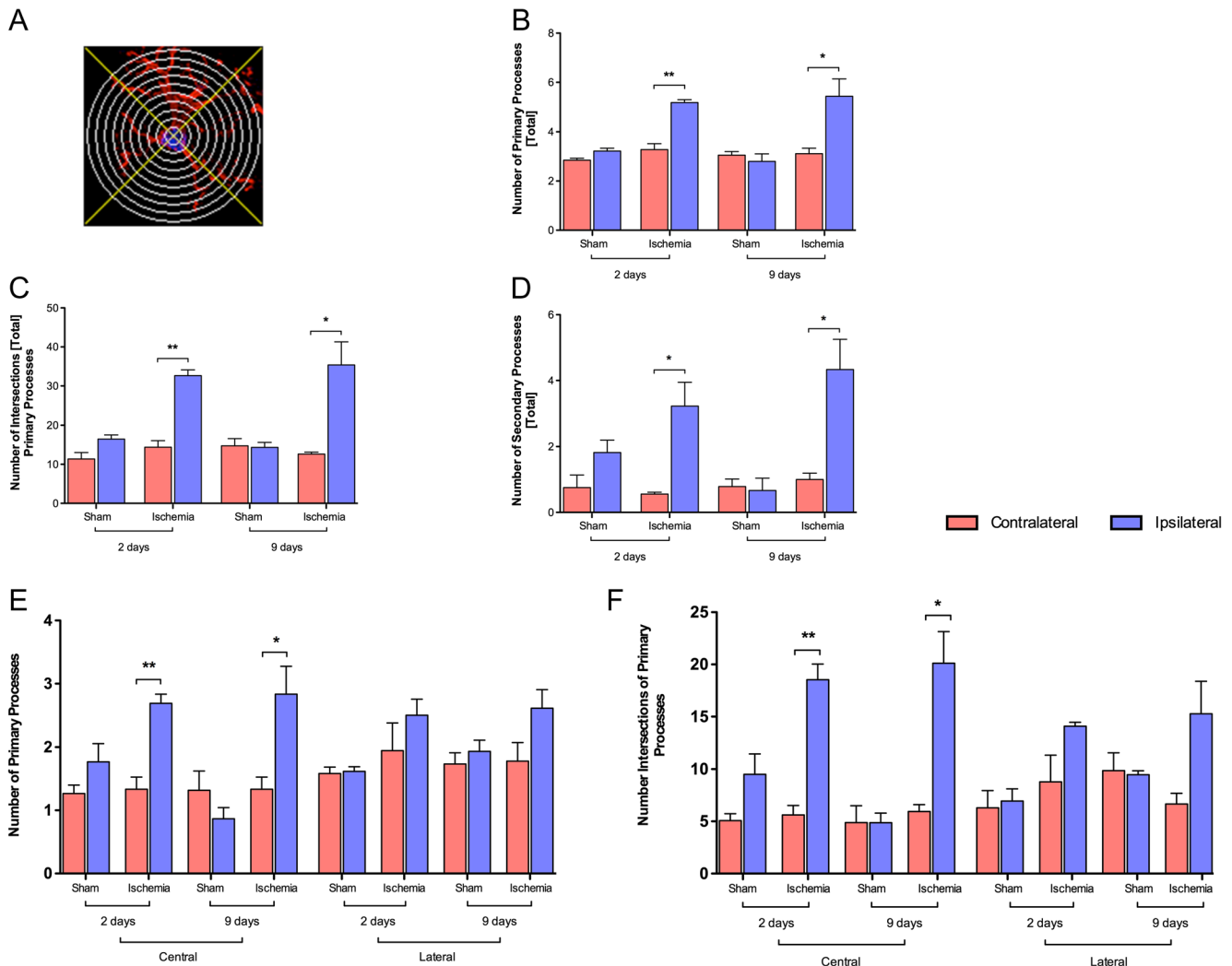


**Fig. 4** Evaluation of cell morphology by Sholl's analysis [48]. **a** Example of an astrocyte with overlaid virtual concentric circles and lines used in Sholl's analysis. **b** Number of total primary processes. **c** Total number of intersections counted for primary processes. **d** Total

number of secondary processes. **e** Number of central and lateral primary processes of astrocytes and **f** intersections. All data are expressed as the means + SEM, \* $P < 0.05$ ; \*\* $P < 0.01$  (one-way ANOVA,  $n = 6$  per group)

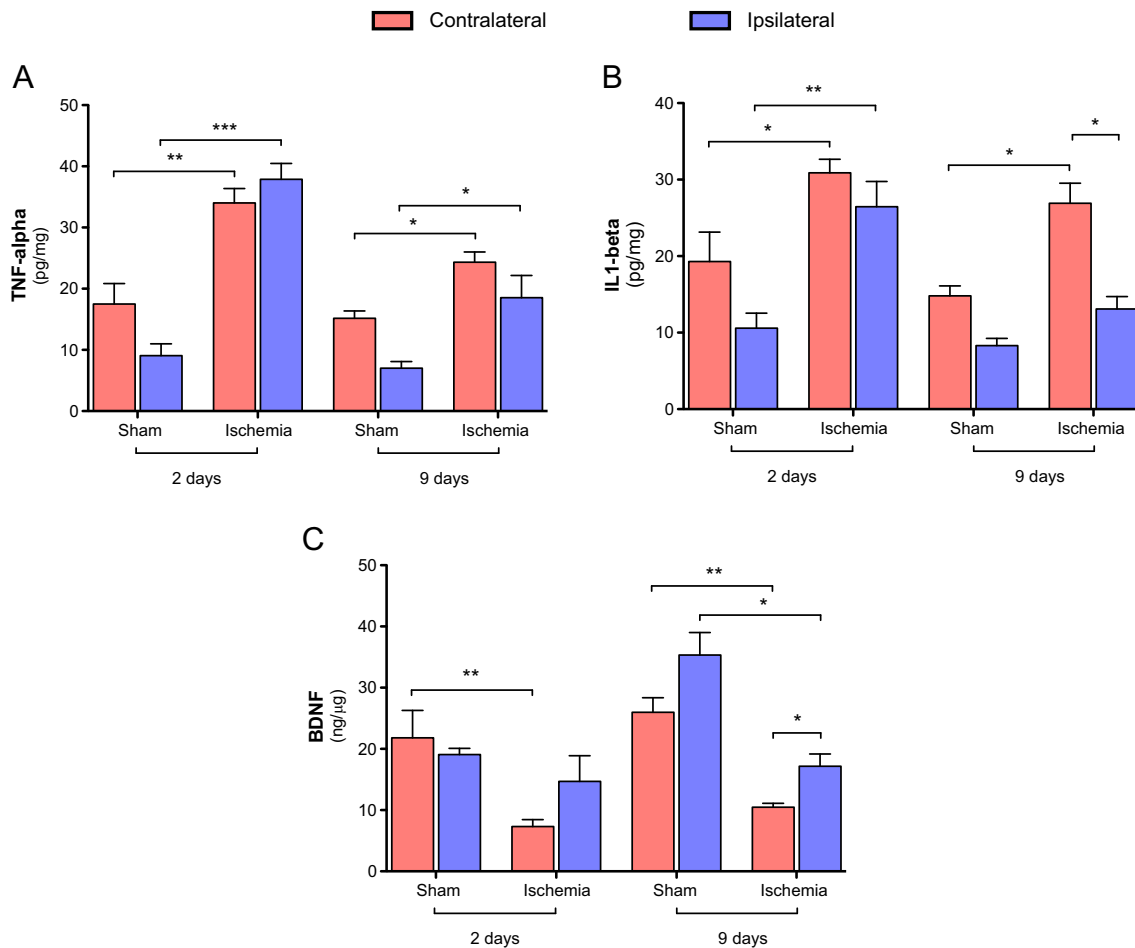


**Fig. 5** Cytokine and trophic factor concentrations in the cerebral cortex after FPI. **a** FPI elevated TNF- $\alpha$  levels in both hemispheres at 2 days, which persisted up to 9 days, and **b** FPI enhanced IL-1 $\beta$  levels. At 2 days, their levels were higher in both cortices; however, only in the contralateral cortex they remained higher at 9 days. **c** FPI diminished BDNF levels in

the contralateral cortex at 2 days and in both hemispheres at 9 days. At the same time point, it was also observed that the ischemic ipsilateral cortex produced more BDNF than the contralateral. All data are expressed as the means + SEM, \* $P < 0.05$ ; \*\* $P < 0.01$ ; \*\*\*\* $P < 0.0001$  (one-way ANOVA,  $n = 6$  per group)

ipsilateral I,  $26.45 + 3.298$ ; S,  $10.58 + 1.976$ ;  $P = 0.0070$ ; 9 days, contralateral I,  $26.90 + 2.621$ ; S,  $14.80 + 1.308$ ;  $P = 0.0145$ ; ipsilateral I,  $13.10 + 1.607$ ;  $P = 0.0109$ ).

FPI decreased BDNF levels in the contralateral hemisphere at 2 days, an effect that persisted up to 9 days (Fig. 5c; 2 days, I,  $7.317 + 1.123$ ; S,  $21.80 + 4.477$ ;  $P = 0.0052$ ; 9 days, I,  $10.47 + 0.6489$ ; S,  $25.97 + 2.395$ ;  $P = 0.0033$ ) and was followed by an ipsilateral decrease in BDNF at 9 days (Fig. 5c; ipsilateral I,  $17.17 + 1.995$ ; S,  $35.33 + 3.670$ ;  $P = 0.0122$ ). Nevertheless, ipsilateral levels of BDNF were still higher than contralateral levels in the ischemia group (Fig. 5c;  $P = 0.0331$ ).

### Lactate Metabolism Is Affected in Both Hemispheres After FPI

Figure 6 shows the significant changes in brain lactate metabolism caused by FPI. Two days following injury,

MCT2 immunocontent was reduced only in the contralateral cortex compared to sham animals (Fig. 6a; contralateral I,  $70.97 + 6.42$ ; S,  $100.0 + 4.40$ ;  $P = 0.0203$ ), an effect that did not persist up to 9 days. In contrast, FPI caused a significant increase in MCT4 protein levels only in the contralateral hemisphere at 2 days post-FPI (Fig. 6b; contralateral I,  $152.9 + 13.92$ ; S,  $100.0 + 9.963$ ;  $P = 0.0363$ ), an effect that persisted up to 9 days post-FPI, when there was a significant increase in MCT4 immunocontent in both hemispheres (Fig. 6b; ipsilateral I,  $293.8 + 56.22$ ; S,  $100 + 25.8$ ;  $P = 0.0351$ ; contralateral I,  $171.1 + 15.67$ ; S,  $100.0 + 10.81$ ;  $P = 0.0202$ ).

FPI caused an increase in lactate oxidation in both hemispheres at 2 days post-FPI compared with the respective hemispheres of the sham group (Fig. 6c; ipsilateral I,  $144.8 + 10.85$ ; S,  $100.0 + 7.39$ ;  $P = 0.0057$ ; contralateral I,  $182.8 + 21.08$ ; S,  $100.0 + 7.35$ ;  $P = 0.0053$ ), an effect that persisted in

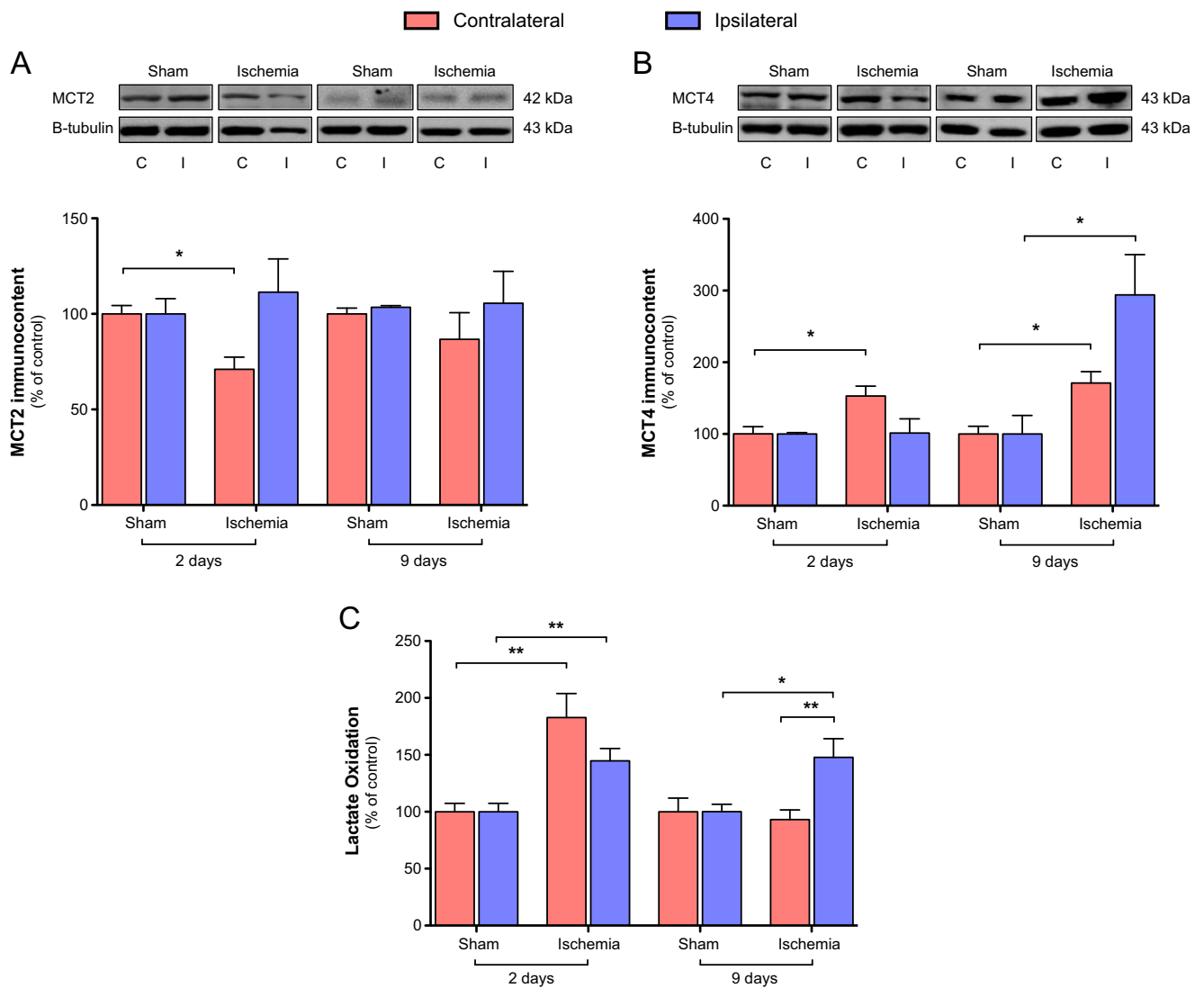


**Fig. 6** Lactate metabolism after FPI. **a** FPI reduced contralateral MCT2 immunocontent and **b** increased contralateral MCT4 immunocontent at 2 days, followed by an increase in both hemispheres at 9 days. **c** FPI increased lactate oxidation in both brain cortices at 2 days. At 9 days, there was still ipsilateral hypermetabolism. Lactate oxidation sham

absolute values (pmol/min/mg of tissue) : 2 days—contralateral =  $0.050 \pm 0.003$  and ipsilateral =  $0.053 \pm 0.003$ ; 9 days—contralateral =  $0.163 \pm 0.021$  and ipsilateral =  $0.181 \pm 0.010$ . All data are expressed as the means + SEM, \* $P < 0.05$ ; \*\* $P < 0.01$ ; \*\*\* $P < 0.001$  (one-way ANOVA,  $n = 5$  per group)

the ipsilateral hemisphere (Fig. 6c; ipsilateral I,  $147.8 \pm 16.33$ ; contralateral I,  $93.09 \pm 8.529$ ;  $P = 0.0082$ ) (Fig. 6c; ipsilateral S,  $100.0 \pm 6.45$ ;  $P = 0.0333$ ).

### Glial Glutamate Metabolism Is Altered by Ischemic Damage

The only effect of FPI on GLAST mRNA was a decrease in the ipsilateral hemisphere at 2 days, which persisted up to 9 days (Fig. 7a; 2 days, ipsilateral I,  $59.68 \pm 9.14$ ; S,  $100.0 \pm 16.09$ ;  $P = 0.05$ ; 9 days, ipsilateral I,  $59.37 \pm 9.57$ ; S,  $100.0 \pm 8.91$ ;  $P = 0.0278$ ; Fig. 7a; ipsilateral I,  $59.68 \pm 9.15$ ; contralateral I,  $102.4 \pm 17.90$ ;  $P = 0.03$ ). FPI also reduced the mRNA content of GLT-1 in both hemispheres at 2 days, an

effect that persisted up to 9 days (Fig. 7b; I,  $51.11 \pm 11.29$ ; S,  $100.0 \pm 16.47$ ;  $P = 0.0328$ ) (Fig. 7b; I,  $64.25 \pm 11.41$ ; S,  $100.0 \pm 9.66$ ;  $P = 0.0379$ ) (Fig. 7b; ipsilateral I,  $34.56 \pm 8.27$ ; S,  $100.0 \pm 18.77$ ;  $P = 0.0227$ ; contralateral I,  $47.98 \pm 11.84$ ; S,  $100.0 \pm 8.80$ ;  $P = 0.0124$ ).

The FPI increased glutamate uptake by cortical slices in both hemispheres at 2 days after injury, an effect that persisted up to 9 days only in the ipsilateral hemisphere (Fig. 7c; ipsilateral I,  $176.5 \pm 26.51$ ; S,  $100.0 \pm 17.58$ ;  $P = 0.0429$ ; contralateral I,  $152.2 \pm 11.66$ ; S,  $100.0 \pm 10.43$ ;  $P = 0.0075$ ) (Fig. 7c; ipsilateral I,  $150.8 \pm 25.10$ ; contralateral I,  $87.81 \pm 7.40$ ;  $P = 0.0229$ ).

Regarding glutamate utilization as an energy substrate, FPI increased the glutamate oxidation 2 days after FPI only in the ipsilateral hemisphere, an effect that persisted up to 9 days

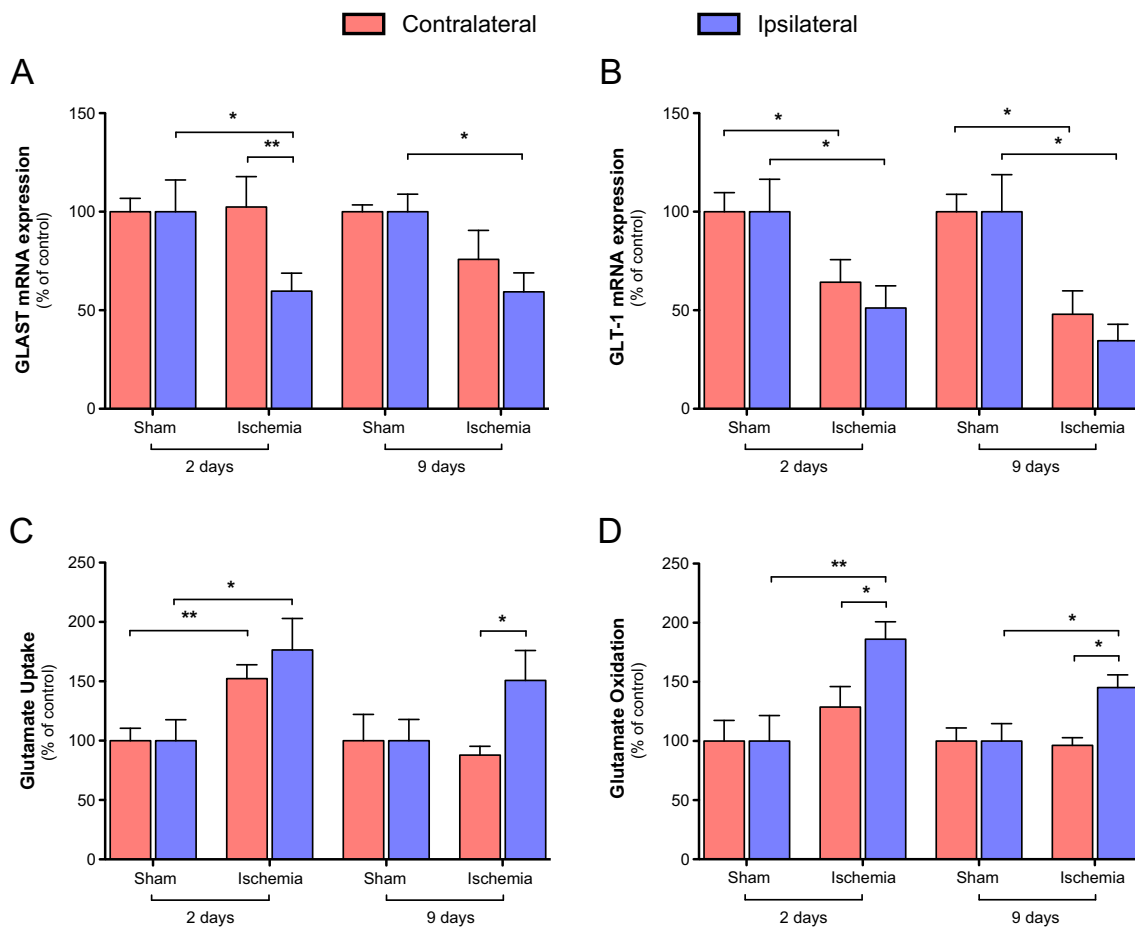


**Fig. 7** Glutamate metabolism after FPI. **a** Ipsilateral GLAST expression was diminished by FPI at both time points. **b** GLT-1 expression in both brain hemispheres was decreased when compared to sham, which persisted up to 9 days post-FPI. **c** FPI induced an increase in glutamate uptake in both brain hemispheres at 2 days; this result persisted up to 9 days only in the ipsilateral hemisphere. **d** Enhanced ipsilateral glutamate oxidation that continued until 9 days post-FPI. Glutamate uptake sham absolute values (pmol/min/mg of protein): 2 days—contralateral =

13.9 ± 1.45 and ipsilateral = 11.9 ± 2.10; 9 days—contralateral = 218.16 ± 48.26 and ipsilateral = 200.48 ± 35.82. Glutamate oxidation sham absolute values (pmol/min/mg of tissue): 2 days—contralateral = 0.070 ± 0.012 and ipsilateral = 0.076 ± 0.016; 9 days—contralateral = 0.037 ± 0.004 and ipsilateral = 0.042 ± 0.006. All data are expressed as the means + SEM. \* $P < 0.05$ ; \*\* $P < 0.01$  (one-way ANOVA,  $n = 6$  per group)

(Fig. 7d; ipsilateral I, 186.0 + 14.69; S, 100.0 + 21.56;  $P = 0.0065$ ) (Fig. 7d; ipsilateral I, 186.0 + 14.69; contralateral I, 128.7 + 17.31;  $P = 0.0275$ ) (Fig. 7d; ipsilateral I, 145.2 + 10.69; S, 100.0 + 014.73;  $P = 0.0279$ ) (Fig. 7d, ipsilateral I, 0145.2 + 10.69; contralateral I, 96.29 + 6.49;  $P = 0.0033$ ).

## Discussion

This study shows the bilateralism of glial modifications following FPI, highlighting the role of energy metabolism adaptations on brain recovery post-ischemia. Focal ischemic injury caused alterations in both the peri-infarct zone in the ipsilateral hemisphere as well as the same region in the intact (contralateral) hemisphere. Some alterations were bilateral, some were present only in the affected

hemisphere (ipsilateral) and some were present only in the intact (contralateral) hemisphere. The investigated alterations refer to bioenergetics, glutamatergic system, reactive astrogliosis, and inflammatory parameters.

**Ipsilateral Hemisphere** Most of the unilateral alterations were found in the ipsilateral hemisphere and persisted until 9 days post-FPI. They include *diminished* in vivo glucose uptake and GLAST expression, followed by increased GFAP gray values, astrocyte reactivity, and glutamate oxidation. In the intact hemisphere, there was a decrease in MCT2 levels, which did not persist.

**Bilateral Alterations** Some of the alterations occurred only at short term (2 days post-FPI), while others persisted until medium term (9 days post-FPI) or only appeared in the later

period. TNF- $\alpha$  levels increased and GLT-1 expression decreased in both brain hemispheres on the cortical ischemic cluster 2 and 9 days post-FPI. In the short term, IL-1 $\beta$  levels were increased in both ipsilateral and contralateral clusters, but this alteration only persisted in the contralateral cortex at 9 days. Lactate oxidation was likely increased 2 days post-FPI in both brain hemispheres, but only the ipsilateral cluster was higher at 9 days. MCT4 and BDNF showed enhanced and diminished levels, respectively, bilaterally at 9 days. Interestingly, both alterations were present 2 days post-FPI, but only in the contralateral hemisphere. This may indicate that there are some adaptations that occur first in the intact hemisphere. Our results provide evidence that focal ischemic injury causes brain bilateral metabolic modulations that may play a role in brain recovery and/or long-lasting adaptations.

Importantly, we demonstrated that the tissue around the lesion (cerebral cortical cluster) was capable of taking up and oxidizing more energy substrates, despite a lower perfusion, and that cytokines and trophic factors were altered in both hemispheres, contributing to the idea that the brain regions analyzed are connected. In addition, our data provide evidence that focal ischemic injury causes metabolic modulations in the ipsilateral hemisphere that persist up to medium term and may play a role in brain recovery and/or long-lasting adaptations.

The expansion of the infarct zone at the cost of viable brain tissue is the “natural” dynamic of permanent vessel occlusion. Nevertheless, some areas can spontaneously recover [53], as we observed in vivo in the micro-PET analysis and ex vivo with TTC staining 9 days following FPI. These results show that the infarcted area recovered its metabolic activity and could indicate ongoing angiogenesis or even migration of cellular progenitors and/or their proliferation [54]. However, metabolic recovery of the infarcted zone did not lead to functional motor improvement, as observed in the cylinder test. Takatsuru et al. [10] demonstrated that functional compensation by the contralateral cortex occurs 1 week after injury; it is only after this period that the animals can use the new synapses formed to recover motor functions. Our results suggest that ipsilateral metabolic recovery might precede this time frame and enable motor improvement.

Previous studies have suggested that GFAP may play a crucial role in neuronal survival after injury, and astrocytes normally have a protective function in the evolution of ischemic brain damage [54–56]. We showed that FPI promotes increased GFAP immunoccontent and numbers of primary processes of astrocytes accounts, thus showing a more radial symmetry of ipsilateral astroglia. Together, these data reflect the reactivity of astrocytes from the FPI group and an important morphological change compared to that observed in astrocytes from the sham rats. Another study involving experimental ischemic stroke in adult mice showed the development of larger infarcts in GFAP $^{-/-}$ Vim $^{-/-}$  mice compared to wild-

type mice [57], suggesting that, in adults, reactive astrocytes are important for the protection of the ischemic penumbral region, mostly through effective elimination of glutamate and reactive oxygen species [57, 58].

As inflammation plays an essential role in the pathogenesis of ischemic stroke and is directly associated with astrocyte reactivity [59, 60], the main pro-inflammatory cytokines were measured to determine the inflammatory profile of glial cells after FPI injury. In this study, TNF- $\alpha$  concentrations were enhanced in both brain hemispheres 2 and 9 days post-surgery. TNF- $\alpha$  receptors in the brain are expressed by neurons and glia, and their activation state as well as the downstream effectors following ischemia are thought to play an important role in determining whether TNF- $\alpha$  will exert a beneficial or harmful effect on the CNS [61]. This dual activity may also depend on the time and progression of the ischemic damage. IL-1 $\beta$  levels, like TNF- $\alpha$ , were higher in both hemispheres compared to the sham group 2 days after the ischemic injury, and these levels remained higher until 9 days after FPI only in the contralateral hemisphere.

BDNF has a protective role in neurodegenerative diseases, including cerebral ischemia [62], since this trophic factor is known to promote anti-inflammatory cytokine release and to downregulate the expression of TNF- $\alpha$  [63]. Our data indicate that the lower content of BDNF might not be able to inhibit TNF- $\alpha$  and IL-1 $\beta$  synthesis, and we therefore observed a high level of pro-inflammatory cytokines in the ischemia group compared to the sham group. BDNF is also considered a potent and beneficial modulator of neuronal functions [64].

Expression of MCTs is regulated at both the transcriptional and translational levels [65]. Robinet and Pellerin [66] demonstrated that MCT2 is regulated by BDNF. As seen previously, our experimental protocol produced a down regulation of BDNF levels in both studied times, mainly in the cerebral cortex of the contralateral hemisphere. This decrease of BDNF in the contralateral cortex was followed by a reduction in MCT2 immunoccontent at 2 days after FPI, presenting a straight regulation on the short-term of this trophic factor and MCT2 [66, 67]. Conversely, under hypoxic conditions, MCT4 expression is upregulated through the transcription factor hypoxia-inducible factor-1 $\alpha$  (HIF-1 $\alpha$ ), since its expression is linked to oxygen tension [30, 68, 69]. In our work, 2 days post-FPI, MCT4 expression was increased only in the contralateral hemisphere. Furthermore, it seems that HIF-1 $\alpha$  is a component of recovery that triggers a response in the intact hemisphere. Wiener and colleagues [70] also reported that brain FPI increases mRNA encoding for HIF-1 $\alpha$  in the penumbra region [71].

One of the most essential roles of astrocytes in the brain is the removal of glutamate from the synaptic cleft via its uptake, which is an energetically expensive process [72–74]. Here, we observed a paradoxical decrease in glutamate transporter expression at the protein level, accompanied by increased

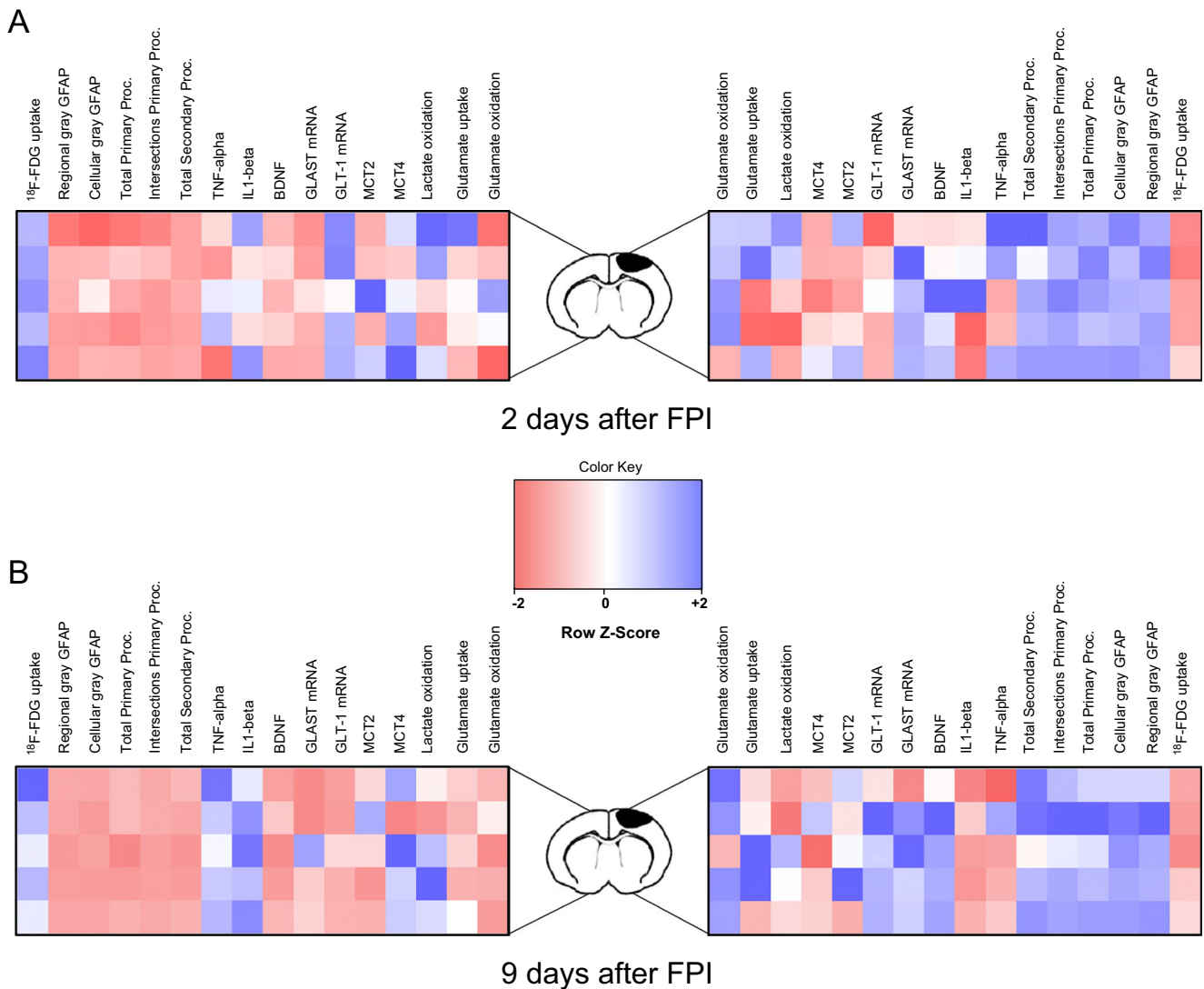


**Fig. 8** Representative cluster of the results in both hemispheres after FPI. The results were analyzed as Z-score values. Z is negative when the sample value is below the mean and positive when above the mean. Each square represents one rat ( $n = 5$  per group)

activity (uptake), which persisted up to medium term. Brain extracellular glutamate concentrations are normally approximately  $2 \mu\text{M}$  [75], but ischemic injury increases glutamate availability in the extracellular space, which might increase the activity of astrocytic glutamate transporters [10]. GLT-1 and GLAST appear to have similar affinities for glutamate, showing a consistent range between  $10.9\text{--}77$  and  $2\text{--}90 \mu\text{M}$ , respectively [75]. Importantly, neither inhibition of astrocyte glutamine synthetase [76] nor the astrocyte TCA cycle [77] are rate limiting for astrocyte glutamate uptake, suggesting that substrate availability may be the mechanism involved in the enhanced glutamate uptake post-FPI in the cortical ischemic cluster.

Previous studies have shown that neurons are directly involved in regulating the expression of both GLT-1 and GLAST [78–80]. Thus, the downregulation of these transporters in this study could be a consequence of glutamate-

induced neuronal death or the reduction of synaptic activity in both brain hemispheres in the analyzed areas. On the other hand, GLAST mRNA expression was diminished in the ipsilateral hemisphere. Interestingly, 2 days following FPI, we identified increased glutamate uptake and lactate oxidation in both ipsi- and contralateral cortices. Nine days after FPI, glutamate and lactate oxidation rates were still elevated, and [ $^{18}\text{F}$ ]FDG uptake was decreased in the ipsilateral cortex. Based on recent evidences [18, 19], it seems that glutamate-derived lactate could be produced and used as an energy source within the brain. However, the precise molecular coupling between glutamate and lactate metabolism remains to be determined.

Overall, our results provide new evidence that astrocytes removed from the affected area, not only those in the affected hemisphere, are adapting some aspects of their metabolism (Fig. 8), potentially contributing to mechanisms that could

attenuate brain damage following ischemic insult. Long-lasting (after 9 days post-FPI) adaptations are under investigation in our group. Specifically, a link between the glutamatergic system and lactate metabolism was observed, which seems to depend on some connectivity between the ipsilateral and contralateral cortices. These significant changes support the hypothesis of metabolic reprogramming occurring after ischemic injury, which appear to promote recovery and adaptation, offering perspectives for new stroke therapeutic targets for clinical application.

**Acknowledgments** This work was supported by the Science Without Borders Program (88881.030387/2013-1), Conselho Nacional de Desenvolvimento Científico e Tecnológico (CNPq), Coordenação de Aperfeiçoamento de Pessoal de Nível Superior (CAPES), Fundação de Amparo à Pesquisa do Estado do Rio Grande do Sul (FAPERGS) e Instituto Nacional de Ciência e Tecnologia para Excitotoxicidade e Neuroproteção (573577/2008-5).

**Compliance with Ethical Standards** All animal experiments were performed in accordance with the National Institutes of Health “Guide for the Care and Use of Laboratory Animals” (NIH publication no. 80-23, revised 1996) and were approved by the Federal University of Rio Grande do Sul Animal Care and Use Committee (process number 26674).

## References

- Kim AS, Johnston SC (2011) Global variation in the relative burden of stroke and ischemic heart disease. *Circulation* 124(3):314–323. doi:10.1161/circulationaha.111.018820
- Go AS, Mozaffarian D, Roger VL, Benjamin EJ, Berry JD, Blythe DJ, Dai S, Ford ES et al (2014) Executive summary: heart disease and stroke statistics—2014 update: a report from the American Heart Association. *Circulation* 129(3):399–410. doi:10.1161/01.cir.0000442015.53336.12
- Dobkin BH (2005) Rehabilitation after Stroke. *N Engl J Med* 352(16):1677–1684. doi:10.1056/NEJMcp043511
- Di Carlo A (2009) Human and economic burden of stroke. *Age Ageing* 38(1):4–5. doi:10.1093/ageing/afn282
- Brouns R, De Deyn PP (2009) The complexity of neurobiological processes in acute ischemic stroke. *Clin Neurol Neurosurg* 111(6):483–495. doi:10.1016/j.clineuro.2009.04.001
- Dimagl U, Endres M (2014) Found in translation: preclinical stroke research predicts human pathophysiology, clinical phenotypes, and therapeutic outcomes. *Stroke* 45(5):1510–1518. doi:10.1161/STROKEAHA.113.004075
- Guadagno JV, Calautti C, Baron JC (2003) Progress in imaging stroke: emerging clinical applications. *Br Med Bull* 65:145–157
- Chollet F, DiPiero V, Wise RJ, Brooks DJ, Dolan RJ, Frackowiak RS (1991) The functional anatomy of motor recovery after stroke in humans: a study with positron emission tomography. *Ann Neurol* 29(1):63–71. doi:10.1002/ana.410290112
- Wittenberg GF, Chen R, Ishii K, Bushara KO, Eckloff S, Croarkin E, Taub E, Gerber LH et al (2003) Constraint-induced therapy in stroke: magnetic-stimulation motor maps and cerebral activation. *Neurorehabil Neural Repair* 17(1):48–57
- Takatsuru Y, Nabekura J, Koibuchi N (2014) Contribution of neuronal and glial circuit in intact hemisphere for functional remodeling after focal ischemia. *Neurosci Res* 78:38–44. doi:10.1016/j.neures.2013.07.004
- Calautti C, Baron JC (2003) Functional neuroimaging studies of motor recovery after stroke in adults: a review. *Stroke; a journal of cerebral circulation* 34(6):1553–1566. doi:10.1161/01.str.0000071761.36075.a6
- Bidmon HJ, Jancsik V, Schleicher A, Hagemann G, Witte OW, Woodhams P, Zilles K (1998) Structural alterations and changes in cytoskeletal proteins and proteoglycans after focal cortical ischemia. *Neuroscience* 82(2):397–420
- Yasuda Y, Tateishi N, Shimoda T, Satoh S, Ogitani E, Fujita S (2004) Relationship between S100beta and GFAP expression in astrocytes during infarction and glial scar formation after mild transient ischemia. *Brain Res* 1021(1):20–31. doi:10.1016/j.brainres.2004.06.015
- Han HS, Yenari MA (2003) Cellular targets of brain inflammation in stroke. *Current opinion in investigational drugs* (London, England: 2000) 4(5):522–529
- Rossi DJ, Brady JD, Mohr C (2007) Astrocyte metabolism and signaling during brain ischemia. *Nat Neurosci* 10(11):1377–1386. doi:10.1038/nn2004
- Carmichael ST (2010) Targets for neural repair therapies after stroke. *Stroke; a journal of cerebral circulation* 41(10 Suppl):S124–S126. doi:10.1161/strokeaha.110.597146
- Zhao Y, Rempe DA (2010) Targeting astrocytes for stroke therapy. *Neurotherapeutics: the journal of the American Society for Experimental NeuroTherapeutics* 7(4):439–451. doi:10.1016/j.nurt.2010.07.004
- McKenna MC (2013) Glutamate pays its own way in astrocytes. *Front Endocrinol* 4:191. doi:10.3389/fendo.2013.00191
- McKenna MC, Sonnewald U, Huang X, Stevenson J, Zielke HR (1996) Exogenous glutamate concentration regulates the metabolic fate of glutamate in astrocytes. *J Neurochem* 66(1):386–393
- Swanson RA, Ying W, Kauppinen TM (2004) Astrocyte influences on ischemic neuronal death. *Curr Mol Med* 4(2):193–205
- Schurr A, Payne RS, Miller JJ, Rigor BM (1997) Brain lactate, not glucose, fuels the recovery of synaptic function from hypoxia upon reoxygenation: an in vitro study. *Brain Res* 744(1):105–111
- Berthet C, Lei H, Thevenet J, Gruetter R, Magistretti PJ, Hirt L (2009) Neuroprotective role of lactate after cerebral ischemia. *Journal of cerebral blood flow and metabolism: official journal of the International Society of Cerebral Blood Flow and Metabolism* 29(11):1780–1789. doi:10.1038/jcbfm.2009.97
- Castillo X, Rosafio K, Wyss MT, Drandarov K, Buck A, Pellerin L, Weber B, Hirt L (2015) A probable dual mode of action for both L- and D-lactate neuroprotection in cerebral ischemia. *Journal of cerebral blood flow and metabolism: official journal of the International Society of Cerebral Blood Flow and Metabolism* 35(10):1561–1569. doi:10.1038/jcbfm.2015.115
- Schurr A, Payne RS, Miller JJ, Tseng MT, Rigor BM (2001) Blockade of lactate transport exacerbates delayed neuronal damage in a rat model of cerebral ischemia. *Brain Res* 895(1–2):268–272
- Berthet C, Castillo X, Magistretti PJ, Hirt L (2012) New evidence of neuroprotection by lactate after transient focal cerebral ischaemia: extended benefit after intracerebroventricular injection and efficacy of intravenous administration. *Cerebrovascular diseases (Basel, Switzerland)* 34(5–6):329–335. doi:10.1159/000343657
- Pierre K, Pellerin L (2005) Monocarboxylate transporters in the central nervous system: distribution, regulation and function. *J Neurochem* 94(1):1–14. doi:10.1111/j.1471-4159.2005.03168.x
- Pierre K, Pellerin L, Debernardi R, Riederer BM, Magistretti PJ (2000) Cell-specific localization of monocarboxylate transporters, MCT1 and MCT2, in the adult mouse brain revealed by double immunohistochemical labeling and confocal microscopy. *Neuroscience* 100(3):617–627
- Rafiki A, Boulland JL, Halestrap AP, Ottersen OP, Bergersen L (2003) Highly differential expression of the monocarboxylate transporters MCT2 and MCT4 in the developing rat brain. *Neuroscience* 122(3):677–688

29. Pellerin L, Bergersen LH, Halestrap AP, Pierre K (2005) Cellular and subcellular distribution of monocarboxylate transporters in cultured brain cells and in the adult brain. *J Neurosci Res* 79(1–2):55–64. doi:10.1002/jnr.20307
30. Rosafio K, Pellerin L (2014) Oxygen tension controls the expression of the monocarboxylate transporter MCT4 in cultured mouse cortical astrocytes via a hypoxia-inducible factor-1 $\alpha$ -mediated transcriptional regulation. *Glia* 62(3):477–490. doi:10.1002/glia.22618
31. Rosafio K, Castillo X, Hirt L, Pellerin L (2016) Cell-specific modulation of monocarboxylate transporter expression contributes to the metabolic reprogramming taking place following cerebral ischemia. *Neuroscience* 317:108–120. doi:10.1016/j.neuroscience.2015.12.052
32. Yu M, Xue Y, Liang W, Zhang Y, Zhang Z (2015) Protection mechanism of early hyperbaric oxygen therapy in rats with permanent cerebral ischemia. *J Phys Ther Sci* 27(10):3271–3274. doi:10.1589/jpts.27.3271
33. Szele FG, Alexander C, Chesselet MF (1995) Expression of molecules associated with neuronal plasticity in the striatum after aspiration and thermocoagulatory lesions of the cerebral cortex in adult rats. *The Journal of neuroscience : the official journal of the Society for Neuroscience* 15(6):4429–4448
34. Giraldi-Guimardes A, Rezende-Lima M, Bruno FP, Mendez-Otero R (2009) Treatment with bone marrow mononuclear cells induces functional recovery and decreases neurodegeneration after sensorimotor cortical ischemia in rats. *Brain Res* 1266:108–120. doi:10.1016/j.brainres.2009.01.062
35. Hansel G, Ramos DB, Delgado CA, Souza DG, Almeida RF, Portela LV, Quincozes-Santos A, Souza DO (2014) The potential therapeutic effect of guanosine after cortical focal ischemia in rats. *PLoS One* 9(2):e90693. doi:10.1371/journal.pone.0090693
36. Hansel G, Tonon AC, Guella FL, Pettenuzzo LF, Duarte T, Duarte MM, Oses JP, Achaval M et al (2015) Guanosine protects against cortical focal ischemia. Involvement of inflammatory response. *Mol Neurobiol* 52(3):1791–1803. doi:10.1007/s12035-014-8978-0
37. Paxinos G, Watson C (1986) *The rat brain in stereotaxic coordinates*. Academic Press, Sydney
38. de Vasconcelos Dos Santos A, da Costa RJ, Diaz Paredes B, Moraes L, Jasmin G-GA, Mendez-Otero R (2010) Therapeutic window for treatment of cortical ischemia with bone marrow-derived cells in rats. *Brain Res* 1306:149–158. doi:10.1016/j.brainres.2009.09.094
39. Swanson RA, Morton MT, Tsao-Wu G, Savalos RA, Davidson C, Sharp FR (1990) A semiautomated method for measuring brain infarct volume. *Journal of cerebral blood flow and metabolism : official journal of the International Society of Cerebral Blood Flow and Metabolism* 10(2):290–293. doi:10.1038/jcbfm.1990.47
40. Liu S, Zhen G, Meloni BP, Campbell K, Winn HR (2009) Rodent stroke model Guidelines for preclinical stroke Trials (1ST Edition). *Journal of experimental stroke & translational medicine* 2(2):2–27
41. Wyckhuys T, Wyffels L, Langlois X, Schmidt M, Stroobants S, Staelens S (2014) The [18F]FDG muPET readout of a brain activation model to evaluate the metabotropic glutamate receptor 2 positive allosteric modulator JNJ-42153605. *J Pharmacol Exp Ther* 350(2):375–386. doi:10.1124/jpet.114.213959
42. Baptista PP, Saur L, Bagatini PB, Greggio S, Venturin GT, Vaz SP, Ferreira Kdos R, Junqueira JS et al (2015) Antidepressant effects of ketamine are not related to (1)(8)F-FDG metabolism or tyrosine hydroxylase immunoreactivity in the ventral tegmental area of Wistar rats. *Neurochem Res* 40(6):1153–1164. doi:10.1007/s11064-015-1576-3
43. Schiffer WK, Mirrione MM, Biegon A, Alexoff DL, Patel V, Dewey SL (2006) Serial microPET measures of the metabolic reaction to a microdialysis probe implant. *J Neurosci Methods* 155(2):272–284. doi:10.1016/j.jneumeth.2006.01.027
44. Zimmer ER, Parent MJ, Leuzy A, Aliaga A, Aliaga A, Moquin L, Schirmacher ES, Soucy JP et al (2015) Imaging in vivo glutamate fluctuations with [(11)C]ABP688: a GLT-1 challenge with ceftriaxone. *Journal of cerebral blood flow and metabolism : official journal of the International Society of Cerebral Blood Flow and Metabolism* 35(7):1169–1174. doi:10.1038/jcbfm.2015.35
45. Thomazi AP, Godinho GF, Rodrigues JM, Schwalm FD, Frizzo ME, Moriguchi E, Souza DO, Wofchuk ST (2004) Ontogenetic profile of glutamate uptake in brain structures slices from rats: sensitivity to guanosine. *Mech Ageing Dev* 125(7):475–481. doi:10.1016/j.mad.2004.04.005
46. Ferreira GC, Tonin A, Schuck PF, Viegas CM, Ceoloto PC, Latini A, Perry ML, Wyse AT et al (2007) Evidence for a synergistic action of glutaric and 3-hydroxyglutaric acids disturbing rat brain energy metabolism. *Int J Dev Neurosci* 25(6):391–398. doi:10.1016/j.ijdevneu.2007.05.009
47. Muller AP, Longoni A, Farina M, da Silveira CK, Souza DO, Perry ML, de Assis AM (2013) Propylthiouracil-induced hypothyroidism during lactation alters leucine and mannose metabolism in rat cerebellar slices. *Experimental biology and medicine (Maywood, NJ)* 238(1):31–36. doi:10.1258/ebm.2012.012255
48. Livak KJ, Schmittgen TD (2001) Analysis of relative gene expression data using real-time quantitative PCR and the 2<sup>(-Delta Delta C(T))</sup> method. *Methods* 25:402–408
49. Mestriner RG, Saur L, Bagatini PB, Baptista PP, Vaz SP, Ferreira K, Machado SA, Xavier LL et al (2015) Astrocyte morphology after ischemic and hemorrhagic experimental stroke has no influence on the different recovery patterns. *Behav Brain Res* 278:257–261. doi:10.1016/j.bbr.2014.10.005
50. Sholl DA (1953) Dendritic organization in the neurons of the visual and motor cortices of the cat. *J Anat* 87(Pt 4):387–406.381
51. Viola GG, Rodrigues L, Americo JC, Hansel G, Vargas RS, Biasibetti R, Swarowsky A, Goncalves CA et al (2009) Morphological changes in hippocampal astrocytes induced by environmental enrichment in mice. *Brain Res* 1274:47–54. doi:10.1016/j.brainres.2009.04.007
52. Cheadle C, Cho-Chung YS, Becker KG, Vawter MP (2003) Application of z-score transformation to Affymetrix data. *Appl Bioinforma* 2(4):209–217
53. Kunz A, Dimagl U, Mergenthaler P (2010) Acute pathophysiological processes after ischaemic and traumatic brain injury. *Best Pract Res Clin Anaesthesiol* 24(4):495–509. doi:10.1016/j.bpa.2010.10.001
54. Carmichael ST (2015) The 3 Rs of stroke biology: radial, relayed, and regenerative. *Neurotherapeutics : the journal of the American Society for Experimental NeuroTherapeutics*. doi:10.1007/s13311-015-0408-0
55. Tanaka H, Katoh A, Oguro K, Shimazaki K, Gomi H, Itoharu S, Masuzawa T, Kawai N (2002) Disturbance of hippocampal long-term potentiation after transient ischemia in GFAP deficient mice. *J Neurosci Res* 67(1):11–20
56. Middeldorp J, Hol EM (2011) GFAP in health and disease. *Prog Neurobiol* 93(3):421–443. doi:10.1016/j.pneurobio.2011.01.005
57. Li L, Lundkvist A, Andersson D, Wilhelmsson U, Nagai N, Pardo AC, Nodin C, Stahlberg A et al (2008) Protective role of reactive astrocytes in brain ischemia. *Journal of cerebral blood flow and metabolism : official journal of the International Society of Cerebral Blood Flow and Metabolism* 28(3):468–481. doi:10.1038/sj.jcbfm.9600546
58. de Pablo Y, Nilsson M, Pekna M, Pekny M (2013) Intermediate filaments are important for astrocyte response to oxidative stress induced by oxygen-glucose deprivation and reperfusion. *Histochem Cell Biol* 140(1):81–91. doi:10.1007/s00418-013-1110-0
59. Muir KW, Tyrrell P, Sattar N, Warburton E (2007) Inflammation and ischaemic stroke. *Curr Opin Neurol* 20(3):334–342. doi:10.1097/WCO.0b013e32813ba151
60. Ansar S, Edvinsson L (2008) Subtype activation and interaction of protein kinase C and mitogen-activated protein kinase controlling



- receptor expression in cerebral arteries and microvessels after subarachnoid hemorrhage. *Stroke; a journal of cerebral circulation*;39. doi:10.1161/STROKEAHA.107.487827
61. Figiel I (2008) Pro-inflammatory cytokine TNF-alpha as a neuroprotective agent in the brain. *Acta Neurobiol Exp* 68(4):526–534
  62. Kiprianova I, Freiman TM, Desiderato S, Schwab S, Galmbacher R, Gillardon F, Spranger M (1999) Brain-derived neurotrophic factor prevents neuronal death and glial activation after global ischemia in the rat. *J Neurosci Res* 56(1):21–27
  63. Jiang Y, Wei N, Zhu J, Lu T, Chen Z, Xu G, Liu X (2010) Effects of brain-derived neurotrophic factor on local inflammation in experimental stroke of rat. *Mediat Inflamm* 2010:10. doi:10.1155/2010/372423
  64. Chen A, Xiong LJ, Tong Y, Mao M (2013) The neuroprotective roles of BDNF in hypoxic ischemic brain injury. *Biomedical reports* 1(2):167–176. doi:10.3892/br.2012.48
  65. Halestrap AP (2013) The SLC16 gene family - structure, role and regulation in health and disease. *Mol Asp Med* 34(2–3):337–349. doi:10.1016/j.mam.2012.05.003
  66. Robinet C, Pellerin L (2011) Brain-derived neurotrophic factor enhances the hippocampal expression of key postsynaptic proteins in vivo including the monocarboxylate transporter MCT2. *Neuroscience* 192:155–163. doi:10.1016/j.neuroscience.2011.06.059
  67. Robinet C, Pellerin L (2010) Brain-derived neurotrophic factor enhances the expression of the monocarboxylate transporter 2 through translational activation in mouse cultured cortical neurons. *J Cereb Blood Flow Metab* 30(2):286–298. doi:10.1038/jcbfm.2009.208
  68. Singh N, Sharma G, Mishra V (2012) Hypoxia inducible factor-1: its potential role in cerebral ischemia. *Cell Mol Neurobiol* 32(4):491–507. doi:10.1007/s10571-012-9803-9
  69. Bergersen LH (2015) Lactate transport and signaling in the brain: potential therapeutic targets and roles in body-brain interaction. *Journal of cerebral blood flow and metabolism : official journal of the International Society of Cerebral Blood Flow and Metabolism* 35(2):176–185. doi:10.1038/jcbfm.2014.206
  70. Wiener CM, Booth G, Semenza GL (1996) In vivo expression of mRNAs encoding hypoxia-inducible factor 1. *Biochem Biophys Res Commun* 225(2):485–488. doi:10.1006/bbrc.1996.1199
  71. Bergeron M, Yu AY, Solway KE, Semenza GL, Sharp FR (1999) Induction of hypoxia-inducible factor-1 (HIF-1) and its target genes following focal ischaemia in rat brain. *Eur J Neurosci* 11(12):4159–4170
  72. Danbolt NC (2001) Glutamate uptake. *Prog Neurobiol* 65(1):1–105
  73. McKenna MC (2007) The glutamate-glutamine cycle is not stoichiometric: fates of glutamate in brain. *J Neurosci Res* 85(15):3347–3358. doi:10.1002/jnr.21444
  74. Kreft M, Bak LK, Waagepetersen HS, Schousboe A (2012) Aspects of astrocyte energy metabolism, amino acid neurotransmitter homeostasis and metabolic compartmentation. *ASN neuro* 4(3). doi:10.1042/an20120007
  75. Anderson CM, Swanson RA (2000) Astrocyte glutamate transport: review of properties, regulation, and physiological functions. *Glia* 32(1):1–14
  76. Rothstein JD, Tabakoff B (1985) Glial and neuronal glutamate transport following glutamine synthetase inhibition. *Biochem Pharmacol* 34(1):73–79
  77. Swanson RA, Graham SH (1994) Fluorocitrate and fluoroacetate effects on astrocyte metabolism in vitro. *Brain Res* 664(1–2):94–100
  78. Gegelashvili G, Danbolt NC, Schousboe A (1997) Neuronal soluble factors differentially regulate the expression of the GLT1 and GLAST glutamate transporters in cultured astroglia. *J Neurochem* 69(6):2612–2615
  79. Swanson RA, Liu J, Miller JW, Rothstein JD, Farrell K, Stein BA, Longuemare MC (1997) Neuronal regulation of glutamate transporter subtype expression in astrocytes. *The Journal of neuroscience : the official journal of the Society for Neuroscience* 17(3):932–940
  80. Schlag BD, Vondrasek JR, Munir M, Kalandadze A, Zelenia OA, Rothstein JD, Robinson MB (1998) Regulation of the glial Na<sup>+</sup>-dependent glutamate transporters by cyclic AMP analogs and neurons. *Mol Pharmacol* 53(3):355–369